# Self-Assembly of an Aspartate-Rich Sequence from the Adenovirus Fiber Shaft: Insights from Molecular Dynamics Simulations and Experiments

**ARTICLE** *in* THE JOURNAL OF PHYSICAL CHEMISTRY B · JANUARY 2014

Impact Factor: 3.3 · DOI: 10.1021/jp409988n · Source: PubMed

THE JOURNAL OF PHYSICAL CHEMISTRY B

Article

pubs.acs.org/JPCB

# Self-Assembly of an Aspartate-Rich Sequence from the Adenovirus Fiber Shaft: Insights from Molecular Dynamics Simulations and Experiments

Phanourios Tamamis,[†] Konstantina Terzaki,[‡,§] Michalis Kassinopoulos,[†] Lefteris Mastrogiannis,[‡,§] Estelle Mossou,[∥,⊥] V. Trevor Forsyth,[∥,⊥] Edward P. Mitchell,[⊥,#] Anna Mitraki,*[,‡,§] and Georgios Archontis*[,†]

[†]Department of Physics, University of Cyprus, 75 Kallipoleos Street, CY1678 Nicosia, Cyprus

[‡]Department of Materials Science and Technology, University of Crete, P.O. Box 2208, GR-71003 Heraklion, Crete, Greece

[§]Institute for Electronic Structure and Laser, FORTH, P.O. Box 1527, GR-71110 Heraklion, Greece

[∥]EPSAM/ISTM, Keele University, Keele, Staffordshire ST5 5BG, United Kingdom

[⊥]Partnership for Structural Biology, Institut Laue Langevin, 6 rue Jules Horowitz, 38042 Grenoble Cedex 9, France

[#]European Synchrotron Radiation Facility, 6 rue Jules Horowitz, 38043 Grenoble Cedex 9, France

Supporting Information

**ABSTRACT:** The self-assembly of short peptides into fibrous nanostructures (such as fibrils and tubes) has recently become the subject of intense theoretical and experimental scrutiny, as such assemblies are promising candidates for nanobiotechnological applications. The sequences of natural fibrous proteins may provide a rich source of inspiration for the design of such short self-assembling peptides. We describe the self-assembly of the aspartate-rich undecapeptide ($NH_3^+$-LSGSDSDTLTV-$NH_2$), a sequence derived from the shaft of the adenovirus fiber. We demonstrate that the peptide assembles experimentally into amyloid-type fibrils according to widely accepted diagnostic criteria. In addition, we investigate an aqueous solution of undecapeptides by molecular dynamics simulations with an implicit (GB) solvent model. The peptides are frequently arranged in intermolecular $\beta$-sheets, in line with their amyloidogenic propensity. On the basis of both experimental and theoretical insights, we suggest possible structural models of the fibrils and their potential use as scaffolds for templating of inorganic materials.

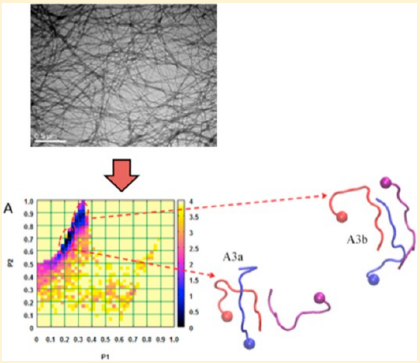


## 1. INTRODUCTION

Synthetic peptides with sequences corresponding to naturally occurring motifs may serve as useful building blocks of self-assembling nanostructures.[1−4] These nanostructures can adopt the form of fibers, tubes, sheets, spheres, and so on and may have important applications in the field of medicine, nanotechnology, and materials science.[5−7] Moreover, their self-assembling mechanisms are of fundamental scientific importance and have been subjected to intense theoretical and experimental scrutiny.[2−4,8,9]

One class of such synthetic peptides has been designed based on sequences corresponding to natural, beta-structured fibrous proteins, such as adenovirus fibers.[1,10] The fiber of adenovirus is a 588 amino acid protein consisting of three domains: a N-terminal tail, a central fibrous shaft, and a globular C-terminal domain.[11] A stable fragment corresponding to residues 319−588 was previously identified and crystallized, revealing a "triple beta-spiral" fold for the shaft domain (residues 319−392).[12] Previous peptide designs were based on sequences extracted from the part of the natural protein with the known crystal structure. These sequences adopted a strand-loop or strand-loop-strand motif in the adenovirus shaft. The corresponding peptides self-assembled into amyloid-type fibers[1] when extracted from the shaft.

Molecular dynamics simulations have provided important insight into the molecular organization of the fibrils, in line with the experimental evidence.[3,4] Moreover, they have assisted in identifying residues exterior to the amyloid fibril core that could be prone to modification. For example, MD simulations have led to the suggestion that residues 1 and 2 are exposed in this way in amyloid fibrils formed from the octapeptide NSGAITIG. On the basis of the insight provided, a variety of amino acids were substituted at these positions without affecting the amyloid-forming core of the peptide. The exposed amino acids have been exploited in studies of the nucleation of inorganic materials. For example, cysteine residues at positions 1 and 2 were found to nucleate the formation of metal nanoparticles.[13] Such metal nanowires templated on peptide

**Received:** October 8, 2013
**Revised:** January 12, 2014
**Published:** January 17, 2014

fibrils are currently being considered for their potential as nanoscale components in future generations of nanodevices.[14] Furthermore, peptides carrying nucleophilic side chains at position 2 (serine, cysteine, threonine) have been found to form fibrils that nucleate the formation of silica nanoparticles. The ability of self-assembling peptide systems to template inorganic materials at the nanoscale level extends to materials such as calcium phosphate (for example, in the form of hydroxyapatite), which are important for biomineralization and hard tissue regeneration.[16−20] We have recently shown that peptides carrying acidic amino acids such as aspartate at position 1 were able to self-assemble into fibrils that templated formation of calcium phosphates on their surface. The mineralized fibrils, when positioned on laser-made scaffolds, were able to support cell adhesion and proliferation of a preosteoblastic cell line and exhibited a statistically significant increase in biomineralization.[21]

In this study we provide experimental and theoretical insight into the self-assembly of an 11-residue peptide from the adenovirus fiber shaft (residues 165−175) with sequence LSGSDSDTLTV. This fragment is located in a part of the shaft with unknown crystal structure and is rich in aspartates and serines. Both amino acids are naturally displayed on the surface of proteins with a role in calcium nucleation and hard tissue formation.[22,23] In particular, the motif D-X, where X is a neutral amino acid, is very frequent in these proteins and is considered to be an important stereochemical requirement for mineralization.[24] Moreover, these acidic proteins are arranged on top of insoluble fibrous macromolecules such as collagen, which provide a structural "framework".[24]

The peptide is found experimentally to self-assemble into amyloid type fibrils, which are structurally characterized using transmission electron microscopy, atomic force microscopy, and X-ray fiber diffraction. To obtain insights into the structural organization of these fibrils, we study the initial stages of the peptide self-assembly by multi$\mu$s replica-exchange molecular dynamics simulations in implicit solvent. The peptides exhibit a tendency to form mainly antiparallel $\beta$-sheets. Analysis of the sheets identifies an off-registered interaction pattern, which is likely to be present in the fibril. The pattern is consistent with a fibrillar width of ∼19 Å, in agreement with the experimentally measured width (20.4 ± 2.5 Å).

## 2. MATERIALS AND METHODS

**Experimental Studies.** *Peptides.* The studied peptide (LSGS) had the sequence $NH_3^+$-**LSGSDSDTLTV**-$NH_2$, corresponding to segments 165−175 of the adenovirus-fiber shaft.[12] The peptide was obtained from Eurogentec (Belgium) and had a purity greater than 95%. Lyophilized peptide powders were dissolved and studied in ultrapure water. For the simulations, the N- and C-terminal groups were chosen for consistency with the experimental conditions.

*Transmission Electron Microscopy.* TEM experiments were performed at the Department of Biology of the University of Crete using a JEOL JEM-100C microscope operating at 80 kV. Eight $\mu$L of peptide solution was placed on a 300 mesh Formvar-coated grid, and after 2 min the excess of the fluid was removed with a filter paper. The samples were negatively stained with 8 $\mu$L of uranyl acetate 1% for 2 min.

*Atomic Force Microscopy.* Drops of the peptide solution were deposited on microscope glass coverslips and were imaged with a Digital Instruments atomic force microscope (Model Multimode with controller Nanoscope IIIa, Veeco). The tapping mode method was used in combination with Si tips.

*X-ray Fiber Diffraction.* Aligned fibers were prepared by drying a drop of peptide solution between glass rods as previously described.[10] X-ray fiber diffraction experiments were performed at the European Synchrotron Radiation Facility (ESRF) in Grenoble (beamline ID14-1). The beam size was 400 × 600 $\mu$m with wavelength 0.934 Å. This experimental arrangement was shown to be optimal for thin amyloid fibrils.[1] Exposure times were 120 s, and images were collected with the detector at 2 Å and detector distance at 205.23 mm. Data processing was carried out using FIT2D[25] and CCP13 software.[26]

**Computational Studies.** All simulations were conducted with the CHARMM program, version c35b2.[27] The analysis was performed with the WORDOM package,[28] the CHARMM program,[27,29] and additional in-house FORTRAN programs.

*Infinite Dilution Simulations in Implicit Aqueous Solution.* These simulations studied an isolated peptide in aqueous solution. The peptide atomic charges, van der Waals, and stereochemical parameters corresponded to the CHARMM19 all-atom force field;[29] the aqueous solvent effects were modeled implicitly by the polar-hydrogen FACTS-generalized Born model.[30] The validity of this model has been established in several recent studies, including Replica Exchange MD simulations of rhodopsin mutants,[31] self-assembly simulations of short peptides from the adenovirus shaft,[3,4] and MD simulations of mechanical unfolding of the 7-ankyrin repeat protein ankyrin.[32] In addition, recent Replica Exchange MD simulations with this model investigated the conformational properties of the HIV-1 gp120 V3 loop;[33] the simulations with the FACTS model in ref 33 showed very good agreement with previous explicit-solvent simulations of the same system[34] and were capable of identifying an HIV-1 gp120 V3 loop conformation that delineated the molecular recognition of CXCR4 by protein HIV-1 gp120. Also, FACTS is used to represent the aqueous environment in the MD protocol of Princeton_TIGRESS[35] and has contributed to the efficient refinement of a wide range of different protein structures. Coulombic interactions were scaled by a dielectric constant $\varepsilon$ = 2 for consistency with the polar-hydrogen FACTS model. A nonpolar solvation free-energy surface term was included, with a surface-tension coefficient of 0.015 kcal/mol/Å$^2$. A 7.5 Å cutoff was used for the nonbonded interactions. Bonds involving hydrogen atoms were constrained to standard values with the SHAKE algorithm,[36] and the equations of motion were integrated by the leapfrog algorithm using a 2.0 fs time step.

To increase sampling efficiency, we used a replica-exchange MD protocol[37−39] of eight replicas with temperatures 283, 300, 318, 336, 356, 377, 403, and 432 K. The temperatures were controlled by the Langevin method, with a friction coefficient of 5.0 ps$^{-1}$ for heavy atoms and 0 ps$^{-1}$ for hydrogen atoms. The simulation length was 1 $\mu$s per replica. We analyzed 10 000 simulation snapshots of the 300 K trajectory, extracted at 100 ps intervals.

*Infinite Dilution Simulations in Explicit Aqueous Solution.* To further check the ability of the implicit model to reproduce the conformational properties of the present peptide, we conducted explicit-solvent simulations under infinite dilution conditions. The peptide atomic charges, van der Waals, and stereochemical parameters were taken from the CHARMM27 all-atom force field,[40] including the CMAP correction.[41] The

water was represented by a modified TIP3P water model.[42,43] The C-terminal of the peptide was blocked by a $CONH_2$ group, in line with experiments. Electrostatic interactions were calculated without truncation by the particle-mesh Ewald method,[44] with a parameter $k$ = 0.5 for the charge screening and sixth-order splines for the mesh interpolations. The Lennard−Jones interactions between atom pairs were shifted to zero at a cutoff distance of 11 Å. The temperature was kept at $T$ = 300 K by a Nosé−Hoover thermostat[45,46] using a mass of 1000 kcal/ps$^2$ for the thermostat. The pressure was maintained at $P$ = 1 atm with a Langevin piston,[47] using a piston mass of 500 a.m.u., a piston collision frequency of 5 ps$^{-1}$, and a piston bath temperature of 300 K. The classical equations of motion were integrated by the Leap-Frog integrator using a time step of 2 fs. Bond lengths to hydrogen atoms and the internal geometry of the water molecules were constrained with the SHAKE algorithm to standard values.[36] The efficiency of a similar simulation setup to reproduce peptide properties in line with experiments was demonstrated in the investigation of 13-residue peptides of the compstatin family.[48]

To create the aqueous environment, we placed a single peptide at the center of a pre-equilibrated cubic water box with a length size of 49 Å. We deleted water molecules with oxygen atoms within 2.5 Å of peptide non-hydrogen atoms, yielding a system with 1 peptide and 4050 water molecules. We conducted 20 independent MD simulations, with the peptide initial coordinates taken at 50 ns intervals from the 300 K REMD infinite dilution trajectory in implicit solvent. Prior to each simulation, we subjected the entire system to a 100 step steepest descent minimization, with the peptide heavy backbone atoms harmonically restrained around their initial positions via a force constant of 2 kcal/mol/Å$^2$. Subsequently, we conducted a 500 ps heating simulation, followed by a 500 ps equilibration simulation. At the end of the equilibration phase, we removed the harmonic restraints and continued the simulation for another 4 ns. During this 4 ns production phase, we saved the coordinates every 25 ps. The total simulation length, after merging all 20 trajectories, was 80 ns.

*Self-Assembly Simulations.* We obtained insight into the early stages of self-assembly by implicit-solvent simulations of six peptides in a periodically replicated 109 Å cubic box, modeling a 8.0 mg/mL solution; this concentration is within the range of fiber-forming conditions.

*Force-Field and Simulation Method for Implicit Solvent Simulations.* The peptide and implicit-solvent force-field parameters and the simulation specifications were the same as those in the infinite-dilution implicit-solvent simulations. We conducted replica-exchange simulations using 16 replicas with temperatures 290, 295, 300, 305, 310, 315, 321, 327, 333, 339, 345, 352, 359, 366, 373, and 380 K. Replica exchanges were attempted at 10 ps intervals.

The initial conformations were generated by placing the six monomers in random positions and orientations within the simulation box. The total simulation length at each temperature was 0.80 $\mu$s. Analysis of the conformational properties of the system at 300 K suggested that the probabilities of frequently observed states (e.g., antiparallel/parallel $\beta$-stranded sheets with two to three strands) converged to stable values within 0.2 $\mu$s. Consequently, we treated the first 0.2 $\mu$s as equilibration stage and analyzed the final 0.60 $\mu$s using 60 000 snapshots extracted at 100 ps intervals.

*Secondary Structure Assignment.* The secondary-structure content was computed with the program DSSP.[49] Additional analysis was performed with in-house programs.

*Classification of Conformations Based on Their $\beta$-Sheet Content.* We classified the observed $\beta$-sheet containing structures into states depending on the antiparallel (A), parallel (P), or mixed (M) strand arrangement and the number of strands within each $\beta$-sheet (2−6). A fraction of the observed sheets contained a combination of antiparallel and parallel $\beta$-bridges within the same pair of strands; we denote these sheets as "complex" (C). In all, we observed 19 distinct states (A2, P2, C2, A3, P3, C3, M3, A4, P4, C4, M4, A5, P5, C5, M5, A6, P6, C6, and M6).

*Classification of $\beta$-Sheet Conformations Based on the Alignment of Their Strands.* We assessed the extent of peptide alignment in two- to five-stranded antiparallel states (A3, A4, A5) by the polar-order parameter $P_1$ and the nematic-order parameter $P_2$, defined in eq 1. These parameters are used in the structural characterization of liquid crystals[50−52] and have been employed successfully in simulation studies of peptide aggregation.[3,4,53]

$$P_1 = \frac{1}{N}\sum_{i=1}^{N} \vec{z}_i\vec{d}, \qquad P_2 = \frac{1}{N}\sum_{i=1}^{N} \frac{3}{2}(\vec{z}_i\vec{d})^2 - \frac{1}{2} \tag{1}$$

In eq 1, $N$ is the number of molecules in the simulation and $\vec{z}_i$ is a unit vector along a suitably defined molecular direction; $\vec{d}$ is a unit vector along a preferred direction of alignment, which emerges from the properties of the system.[50] In our calculations, we defined the molecular axis unit vector $\vec{z}_i$ along the line Asp5(N) − Thr10(C), as explained further in the Results.

The parameter $P_1$ distinguishes between parallel ($P_1 \approx 1$ for well-aligned, parallel strands), antiparallel ($P_1 \leq \mathrm{mod}(N,2)/N$ for well-aligned, antiparallel strands), and mixed orientations ($P_1 \leq 1$ to $2/N$ for well-aligned, mixed strands). $P_2$ distinguishes between ordered ($P_2 \approx 1$ for perfect alignment) and disordered conformations ($P_2 < (81/(40\pi N))^{1/2}$ for a system of N peptides[51,52]). We computed $P_1$ and $P_2$ for the states with three to five strands in parallel or antiparallel arrangement with the program WORDOM.[28] We constructed free-energy surfaces of each state from the 2-D probability $P(P_1, P_2)$ and the relation

$$G(P_1, P_2) = -k_B T \ln[P(P_1, P_2)/P_{max}] \tag{2}$$

where $P_{max}$ denotes the maximum probability value of the particular state.

*Classification of Structural Patterns within High-Probability Conformations in the Antiparallel $\beta$-Sheet Families A3, A4, and A5.* To construct a model for the fiber, we analyzed the $\beta$-bridge interactions between adjacent strands in conformations within the free-energy minima of the A3, A4, and A5 free-energy surfaces. We thus identified a number of interaction patterns involving off-registered strand alignments.

## 3. RESULTS AND DISCUSSION

**Experimental Characterization of the Peptide Nanostructures.** All experiments were carried out at 22 °C (295 K). Solutions of the peptide were first investigated by TEM to assess their assembly properties. Figure 1 shows TEM micrographs of peptide solutions at a concentration of 10 mg/mL after incubation for 21 h following negative staining.


dx.doi.org/10.1021/jp409988n | J. Phys. Chem. B 2014, 118, 1765−1774

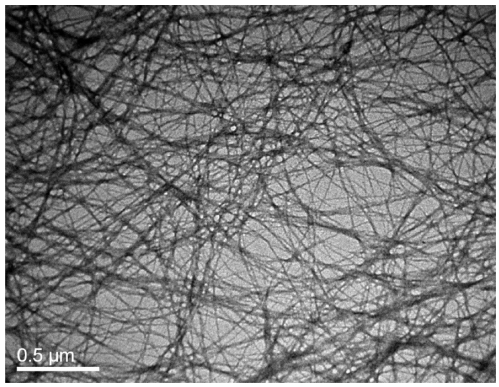


**Figure 1.** TEM image of fibrils formed after incubation for 21 h in water at a concentration of 10 mg/mL. Negative stain with uranyl acetate was used.

Straight, nonbranched fibrils were observed with lengths reaching up to several micrometers and widths ranging from 10 to 40 nm. X-ray fiber diffraction patterns recorded from aligned samples formed from these solutions shows reflections at 4.7 Å on the meridian and 9.9 Å on the equator (Figure 2). These

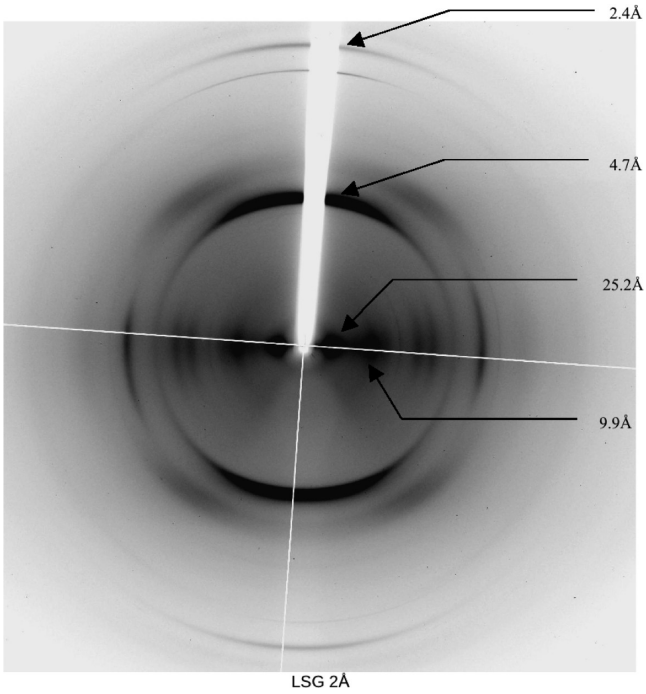


**Figure 2.** X-ray fiber diffraction of fibrous stalks showing the characteristic meridional reflection at 4.7 Å and equatorial reflection at 9.9 Å.

reflections are characteristic of the cross-beta structure and correspond to the hydrogen-bonding distance between beta-strands (4.7 Å) and to intersheet packing distance (9.9 Å).

These results provide strong evidence that the newly designed peptide is able to self-assemble into amyloid-type fibrils, as assessed by the above widely accepted diagnostic criteria.

We subsequently sought to determine the dimension of the protofibril, that is, the "thinnest" fibril formed after the onset of assembly. We therefore measured the dimensions of the fibrils formed at early time points as soon as they become detectable by AFM.

The upper plot of Figure 3 shows fields taken after 1 h of incubation and subsequent deposit on a glass coverslip surface. Short fibrils can be seen along with nonfibrillar objects, probably corresponding to prefibrillar assembly intermediates. The measured heights of the fibrils were 20.4 ± 2.5 Å. (18 objects were measured.) Fully "mature" fibrillar bundles at this concentration are subsequently observed after 7 days of incubation, corresponding to further association of "protofibrils" (lower plot of Figure 3).

**Computational Study of the Early Self-Assembly Stages.** *Infinite Dilution Simulations.* Residue secondary-structure probability profiles corresponding to the implicit-solvent simulations at infinite dilution are shown in the upper left panel of Figure 4 A. The dominant conformation has disordered N- and C-terminal ends and frequently observed fused $\beta$-turns/bends in the segment 3−9. The 6−10 segment adopts helical conformations with ∼20% probability. Intramolecular $\beta$-sheets (mainly isolated $\beta$-bridges between residues Ser2 and Ser6) are also observed with low frequency (∼10%). A representative structure (resulting from cluster analysis of the main-chain Ca atoms with 1.2 Å cutoff) is shown in the upper right panel of Figure 4.

The validity of the employed polar-hydrogen FACTS[30] implicit-solvent model has been established in studies of a diverse set of systems.[3,4,31−33,35] To check the ability of this model to reproduce the conformational properties of the present peptide, we also conducted 80 ns explicit-solvent simulations under infinite dilution conditions, as described in the Methods. The resulting secondary-structure profile (Supplementary Figure SF1 in the Supporting Information) is very similar to the implicit-solvent profile of Figure 4 A, supporting the validity of the model.

*Finite Dilution Simulations.* To obtain insight into early self-assembly stages, we conducted implicit-solvent replica-exchange simulations of a six-peptide system, modeling an 8.0 mg/mL aqueous solution (see Methods).

**Structural Characterization of the Aggregate.** The lower left panel of Figure 4 shows the average secondary structure profile at 300 K. As in the infinite-dilution simulations, the N- and C- terminal residues are mainly disordered. The bend/turn propensity around residue Ser6 is somewhat higher in the finite-dilution simulations due to the fact that a portion (∼8%) of intermolecular $\beta$-sheets contain peptides in a U-shaped ($\beta$-hairpin or $\beta$-turn) conformation. The lower right panel of Figure 4 shows a typical strand conformation in antiparallel sheets with three to five strands.

Segments 7−10 (mainly) and 2−5 (to a smaller extent) are engaged in intermolecular $\beta$-sheets. In antiparallel $\beta$-sheets with three or more strands, interactions between segments 7 and 10 of adjacent strands account for ∼67% of conformations, and interactions between segments 7 and 10 of one strand and segments 2 and 5 of an adjacent strand account for the remaining ∼33%. In parallel $\beta$-sheets with at least three strands, segments 7−10 of one strand prefer to interact with segments 2−5 of an adjacent strand in ∼67% of conformations.

The $\beta$-sheets of the hexamer system can be conveniently classified by the number and orientation of their constituent strands. In the replica exchange simulations of the hexamer, we observed the formation of $\beta$-sheets with two to six strands in antiparallel (A), mixed (M), or parallel (P) orientations. In a small fraction of $\beta$-sheets, adjacent strands formed simulta-


dx.doi.org/10.1021/jp409988n | J. Phys. Chem. B 2014, 118, 1765−1774

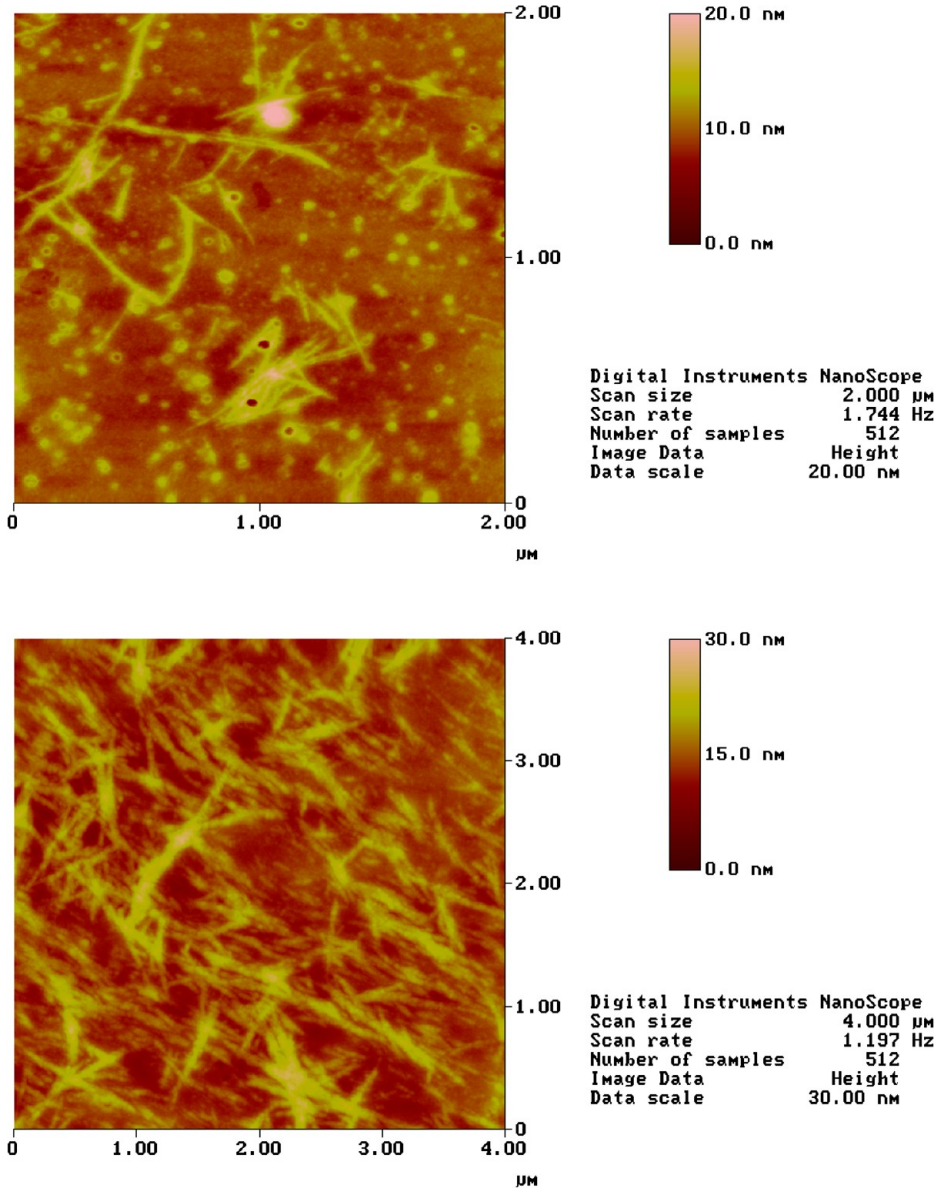


**Figure 3.** Upper plot: AFM image of peptide fibrils formed after 1 h of incubation in water at a concentration of 1 mg/mL. Lower plot: AFM image of peptide fibrils formed after 1 week of incubation in water at a concentration of 1 mg/mL.

neously parallel and antiparallel $\beta$-bridges; we classified such sheets as "complex" (C). Overall, we observed 19 distinct $\beta$-sheet types (A2, P2, C2, A3, P3, C3, M3, A4, P4, M4, C4, A5, P5, C5, M5, A6, P6, M6, and C6). In the employed (XJ) notation, the letter X (A, P, C, or M) denotes the strand orientation, and the integer J (2−6) denotes the number of strands in the sheet; for example, M3 denotes a three-stranded $\beta$-sheet, with its strands in mixed orientation.

Supplementary Figure 2 in the Supporting Information displays running averages of the formation probabilities (%) for all states at 300 K. The most populated states involve sheets with two to three strands; more extended sheets (up to six strands) are also present, reflecting the amyloidogenic potential of the peptide. Antiparallel sheets are more populated with respect to parallel or mixed sheets with the same number of strands, suggesting that the antiparallel is the most likely strand orientation in the fiber. The probabilities of sheets with two to three strands begin to converge to stable values after 250 to 300 ns. The probabilities of more extended states (four to six strands) do not reach convergence within the simulation length (800 ns per replica). Nevertheless, the purpose of these simulations was not to compute accurate probabilities for each conformational state but to sample a representative ensemble of structures that will provide insight into the conformational properties of the fibril. On the basis of the available information, as shown later, we were able to construct a plausible and robust model for the fibril structure.

*Free-Energy Landscapes using Polar and Nematic Order Parameters.* To identify structural patterns likely to exist in the fiber, we focused on antiparallel sheets, which were associated with the highest formation probabilities. Parallel sheets were less populated and more disordered, as suggested by analysis of their $P_1/P_2$ parameters (map not shown); mixed or complex sheets (states MX, CX) lacked the symmetry expected in fibril structures and could not be easily exploited in a construction of a plausible structural model.

As shown in other studies, the degree of molecular alignment in systems with structural order, such as liquid crystals[50−52] and


dx.doi.org/10.1021/jp409988n | J. Phys. Chem. B 2014, 118, 1765−1774

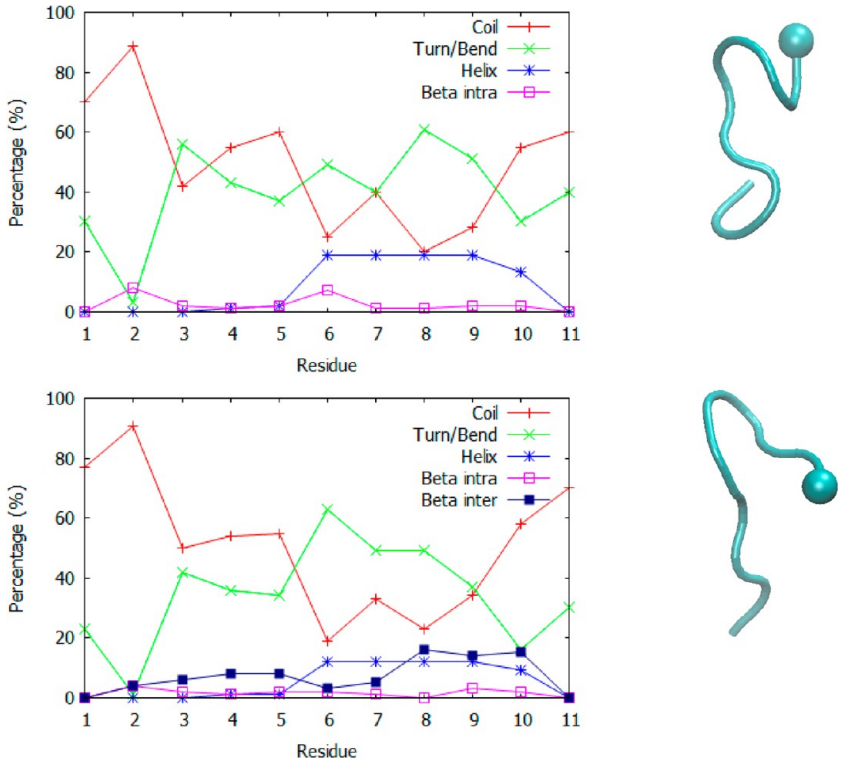


**Figure 4.** Residue secondary-structure probability profiles and representative conformations, resulting from the implicit-solvent MD simulations under infinite-dilution (upper plot) and finite-concentration conditions (lower plot) at 300 K.

nanostructure-forming peptides,[3,4,53] can be quantified with the aid of the order parameters $P_1$ and $P_2$, defined in eq 1 of the Methods. For a system of N molecules, the nematic order parameter $P_2$ distinguishes between well-ordered ($P_2 \approx 1$ for perfect molecular alignment) and disordered conformations ($P_2 < (81/(40\pi N))^{1/2}$[51,52]). The polar-order parameter $P_1$ distinguishes between parallel ($P_1 \approx 1$), antiparallel ($P_1 \approx \mathrm{mod}(N,2)/N$), and mixed orientations (various values $\leq 1$ to $2/N$).

In our hexamer simulations, the majority of $\beta$-sheets comprise a subset of the peptides, with the remaining peptides arranged in random positions and orientations with respect to the sheets. Consequently, the $P_1$ and $P_2$ values of the entire hexamer are largely affected by the variety of conformations and relative alignments of peptides not in sheets. Because our motivation was to identify emergent structural patterns in the $\beta$-sheets, we did not employ the $P_1/P_2$ analysis to the entire hexamer but to the subset of antiparallel sheets with at least one internal strand (states A3, A4, and A5). To accomplish this, we extracted from the hexamer snapshots the coordinates of antiparallel sheets with three to five strands and joined them into separate trajectories; we then evaluated the $P_1$ and $P_2$ values for all snapshots in each trajectory and constructed the corresponding 2-D probabilities and free-energy surfaces via eq 2.

The $P_1$ and $P_2$ definitions contain a unit vector $\vec{z}_i$ that points along the direction of a suitably defined molecular axis (eq 1). As previously explained (see Figure 4 and the accompanying discussion), in our simulations the peptide main chains tended to form a turn around residue 6 and to engage in antiparallel $\beta$-sheets mainly via their moieties 7−10. This is shown in more detail below, when we analyze the interaction patterns of adjacent strands in the antiparallel sheets. For these reasons, we defined vector $\vec{z}_i$ along the line Asp5(N)−Thr10(C). Definitions of $\vec{z}_i$ that included the moiety 1−4 did not well reproduce the strand direction (due to the tendency of peptides to turn around residue 6) and produced poor results.

Figure 5 shows free-energy surfaces (FESs) for states A3, A4, and A5 constructed from the corresponding 2-D probabilities $P(P_1, P_2)$; the properties of the most important regions are summarized later.

Perfectly aligned antiparallel sheets with three strands (A3) have a polar-order parameter $P_1 \approx 1/3$ and a nematic order parameter $P_2 \approx 1.0$. ($P_2$ values below 0.46 correspond to random alignment, as explained in the Methods section.) The A3 FES (Figure 5A) contains two neighboring minima. Representative conformations are also included in Figure 5 A. Both minima correspond to conformations with antiparallel ($P_1 \approx 1/3$) and fairly well-ordered strands ($P_2 > 0.55$), with the structures in global minimum A3a being somewhat less ordered relative to the ones of A3b.

Perfectly aligned antiparallel four-stranded sheets (A4) have $P_1 \approx 0$ and $P_2 \approx 1$ (values $P_2 < 0.40$ indicate a random strand alignment for $n = 4$). The computed FES of A4 (Figure 5B) contains a single global minimum (A4a) with reasonably ordered structures ($P_2 > 0.5$; $0.30 < P_1 < 0.45$). A representative conformation is shown in Figure 5B. In the case of five-stranded antiparallel $\beta$-sheets, perfect alignment is indicated by values $P_1 \approx 1/5$, $P_2 \approx 1$. ($P_2 > 0.36$ is needed for a nonrandom alignment when $n = 5$.) The computed FES of A5 (Figure 5C) contains a global minimum (A5a) with $P_2$ in the range 0.2 to 0.4 and $P_1$ in range 0 to 0.15. Thus, these sheets are not well ordered; a representative conformation is shown in Figure 5C.

*Construction of a Structural Model for the Fibril.* Because of the small size of the simulated system and the limited duration of the runs ($\sim$ 12.8 $\mu$s for all 16 replicas), the present


dx.doi.org/10.1021/jp409988n | J. Phys. Chem. B 2014, 118, 1765−1774

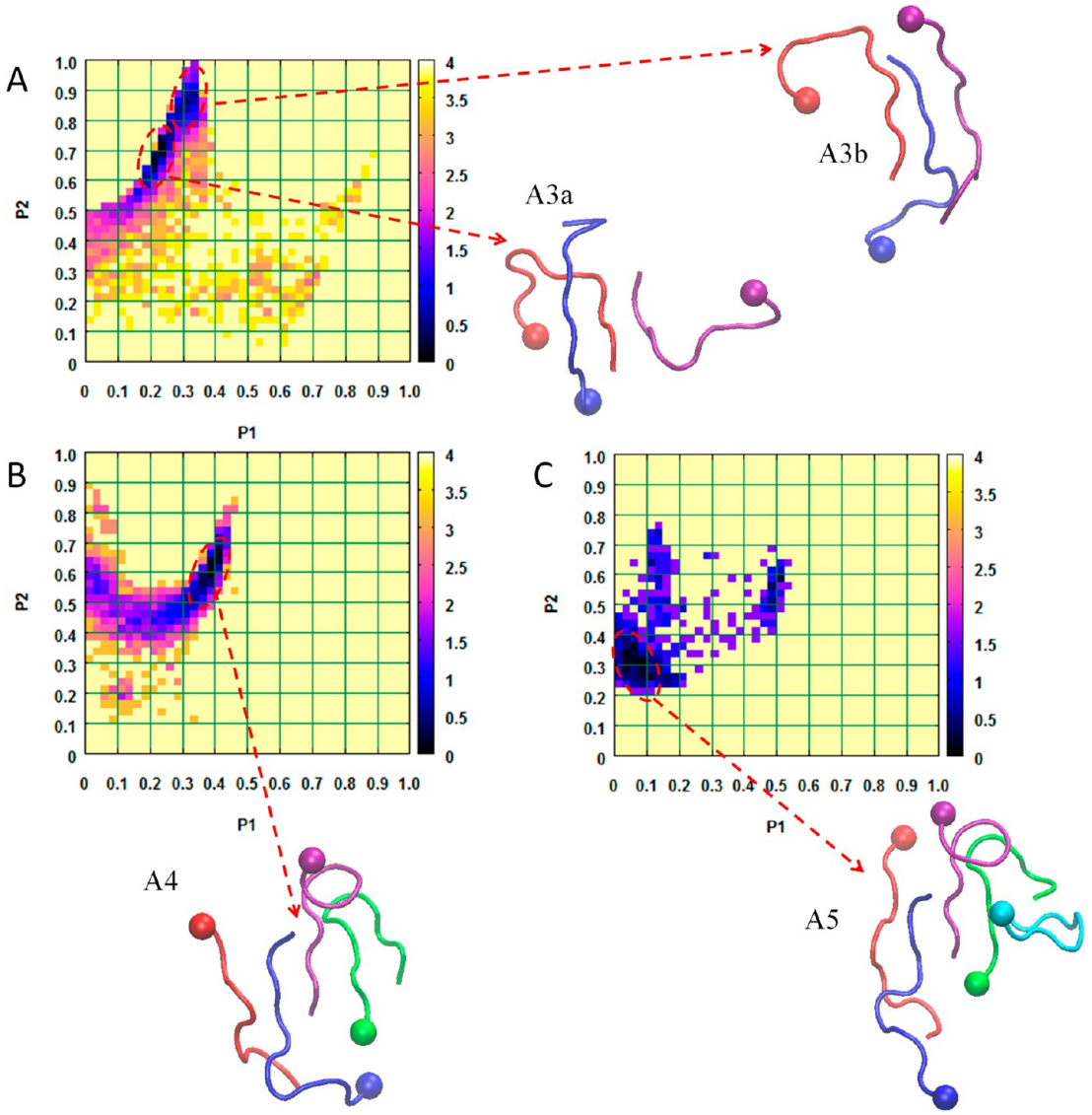


**Figure 5.** Free-energy surfaces (FESs) for antiparallel sheets with three (A), four (B), or five strands (C). The surfaces are constructed from the 2-D probabilities of order parameters $P_1$ and $P_2$ (see text). Representative structures from the FES minima are also shown.

simulations probe only the early stages of aggregation. The simulated system (six peptides in implicit solvent) tends to assemble into aggregates with an ellipsoidal shape, which maximizes the number of intra- and intermolecular nonpolar and polar contacts. This tendency prevents the formation of well-ordered sheets. The degree of strand alignment decreases with the complexity (number of participating strands) of the $\beta$-sheets. Nevertheless, certain patterns of interaction between neighboring strands emerge from the simulations and may also be present in the fibrillar structures. To identify such patterns, we focused on antiparallel $\beta$-sheets with three to five strands (basins A3a, A3b, A4a, and A5a in Figure 5). Two-stranded sheets were omitted because they lack an internal strand, and six-stranded sheets were omitted because they were very infrequently observed.

Probability maps of $\beta$-bridge interactions among adjacent strands are displayed in Figure 6. For each family, the results are averaged over pairs of adjacent strands. Each off-diagonal line corresponds to a distinct off-register antiparallel pattern of interactions between neighboring strands, indicated by an arrow; the number above the arrow denotes the average number of simultaneously participating residues/peptide in $\beta$-bridges.

In families A3a and A3b (Figure 6A,B), we observe four off-register patterns (respectively, denoted as A3a-1 to A3a-4 and A3b-1 to A3b-4). Families A4a and A5a (Figure 6C,D) contain two more patterns (respectively, A4−5 to A4−6 and A5−5 to A5−6). Statistics of all interaction patterns and representative conformations are discussed in the Supporting Information.

To further assess the likelihood of these patterns to be present in the fiber, we asked the following question: could any of the patterns be propagated (by repetition of the corresponding strand dimer) and create an infinite model? We set the following criteria for a satisfactory fiber model: (i) It should be as symmetric as possible (i.e., the individual strands should have similar conformations). (ii) Strand replication (with strand conformations typical of families A3a, A3b, A4, and A5) should not create large steric conflicts between adjacent strands. (iii) Any new $\beta$-bridge interactions that appear in the infinite model should have been observed in the simulations with non-negligible probability.


dx.doi.org/10.1021/jp409988n | J. Phys. Chem. B 2014, 118, 1765−1774

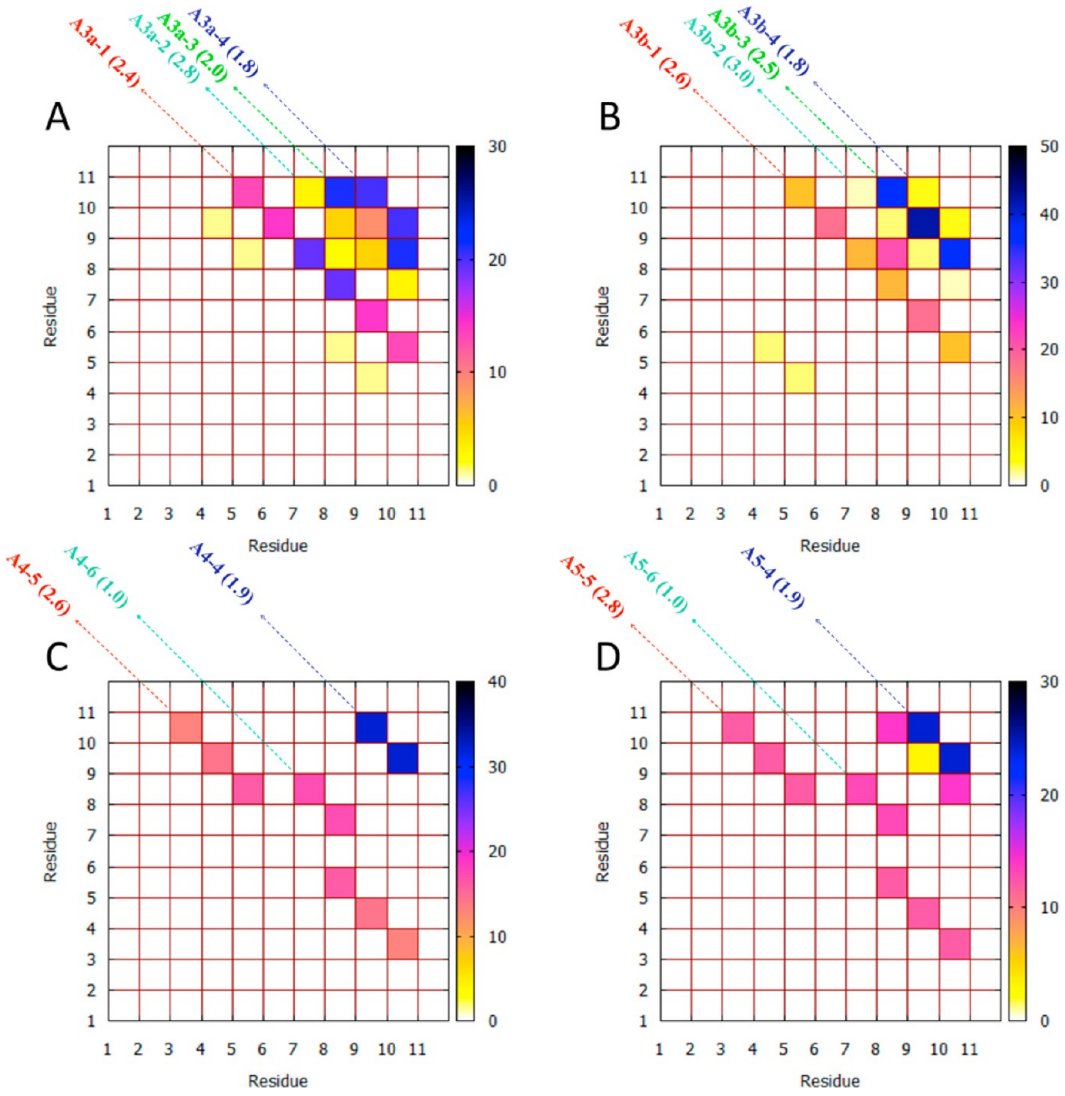


**Figure 6.** Probability maps of the $\beta$-bridges observed in conformations from the FES basins of Figure 5: (A) Basin A3a, (B) Basin A3b, (C) Basin A4, and (D) Basin A5. The arrows indicate characteristic (mainly off-register) antiparallel patterns of interactions between neighboring strands. (See the text and Supporting Information.) The numbers above the arrows denote the average number of simultaneously present residues/peptide in $\beta$-bridges.

Patterns 3 and 5 contain a combination of "I"- and "U"-shaped strand conformations (see Supporting Information) and do not fulfill criterion (i). Moreover, the length of U-shaped conformations is much smaller (~14 Å) than the experimentally estimated fibril length (20.4 ± 2.5 Å), thus indicating that U-shaped conformations are not likely to occur in the naturally occurring fibrils. In patterns 1, 3, 5, and 6, the construction of an infinite model necessitates the introduction of new $\beta$-bridges that were not observed in the finite-concentration simulations. (See the Supporting Information.) Hence, these patterns are inconsistent with criterion (ii).

The remaining two patterns (2 and 4) fulfill all criteria. Pattern 2 involves interactions between segments Asp7 and Thr10 of adjacent strands and has the highest average number of residues/monomer in $\beta$-bridges (2.8 in Figure 6A and 3.0 in Figure 6 B). It is off-registered by five residues and has a six-residue overlap between adjacent strands; the width of the resulting structural model (~19 Å) is within the experimental values (20.4 ± 2.5 Å). This pattern is the most likely to occur in the nanostructure.

Pattern 4 involves interactions between segments 9 and 10 of adjacent strands. It has a smaller average number of interacting residues/monomer in $\beta$-bridges (1.8 to 1.9). It is associated with an off-registered arrangement by seven residues, which yields a much larger fiber diameter (24.7 ± 4.0 Å) than the experimental estimate. For these reasons, this pattern is less likely to occur in the fiber.

## 4. CONCLUSIONS AND PERSPECTIVE

We used transmission electron microscopy, atomic force microscopy, X-ray fiber diffraction, and MD simulations to study the self-assembly of an 11-residue sequence (LSGSDSDTLTV) from the fiber shaft (residues 165−175) of the adenovirus. The peptide self-assembles into amyloid-type fibrils with a width of 20.4 ± 2.5 Å. The MD simulations suggest that the peptide strands are arranged in antiparallel orientation in the fiber and identify an off-registered $\beta$-bridge interaction pattern that is likely to be present in the fiber.

The peptide sequence is rich in aspartates and serines, which are frequent in proteins implicated in calcium nucleation and


dx.doi.org/10.1021/jp409988n | J. Phys. Chem. B 2014, 118, 1765−1774

hard tissue formation.[22,23] Furthermore, it was chosen for study due to its internal S-D-S-D sequence, a frequent sequence motif encountered in proteins implicated in biomineralization.[24] The ability of the peptide to self-assemble into amyloid fibrils, as proven by the experiments, provides (1) an insoluble structural framework that (2) displays aspartate side-chains on surface-exposed beta-bridges, as suggested by the MD insights. Therefore, the combination of both structural and functional requirements in one self-assembled entity should presumably fulfill the necessary conditions for calcium nucleation. Preliminary experiments confirm the calcium nucleation ability of the peptide fibril scaffolds. In future experiments and simulations we plan to address the interactions of calcium ions with the fibrils formed by this peptide.

## ■ ASSOCIATED CONTENT

### Supporting Information

Peptide residue secondary-structure profile from simulations under infinite dilution conditions, the running average of formation probabilities for the 19 $\beta$-sheet states discussed in the main text, as well as figures and statistics of $\beta$-bridges between adjacent strands in antiparallel $\beta$-sheets. This material is available free of charge via the Internet at http://pubs.acs.org.

## ■ AUTHOR INFORMATION

### Corresponding Authors

*Anna Mitraki: Tel: +30 2810394095. E-mail: mitraki@materials.uoc.gr.

*Georgios Archontis: Tel: +357 22 89 28 22. E-mail: archonti@ucy.ac.cy.

### Notes

The authors declare no competing financial interest.

## ■ ACKNOWLEDGMENTS

We thank an anonymous referee for constructive comments. All simulations were conducted in Biophysics clusters at the University of Cyprus. G.A. and P.T. acknowledge support from the Infrastructure Upgrade grant ANAVATHMISI/0609/11 "*Folding and Nanostructure Formation by Biologically-inspired Peptide Sequences From Natural Fibrous Proteins: Insights From Highly-Intensive Computational Studies*" of the Cyprus Research Promotion Foundation, which is cofunded by the European Regional Development Fund. P.T. acknowledges financial support from the University of Cyprus grant "*Computational Investigation of Peptide Sequences from the Adenovirus and Reovirus Fibre Shaft: Insights on the Self-assembly of Peptide-based Nanostructures and the Stability of the Triple-$\beta$ Spiral Fold*". K.T. was supported by the Greek General Secretariat for Research and Technology grant Herakleitos II (Grant number 10.74.11.01). V.T.F., E.M., and E.P.M. acknowledge support from the CRISP consortium funded by the European Commission under the seventh Framework Programme Grant Agreement 283745

## ■ REFERENCES

(1) Papanikolopoulou, K.; Schoehn, G.; Forge, V.; Forsyth, V. T.; Riekel, C.; Hernandez, J. F.; Ruigrok, R. W. H.; Mitraki, A. Amyloid Fibril Formation From Sequences of a Natural Beta-structured Fibrous Protein, the Adenovirus Fiber. *J. Biol. Chem.* **2005**, *280*, 2481−2490.

(2) Tamamis, P.; Adler-Abramovich, L.; Reches, M.; Marshall, K.; Sikorski, P.; Serpell, L.; Gazit, E.; Archontis, G. Self-Assembly of Phenylalanine Oligopeptides: Insights from Experiments and Simulations. *Biophys. J.* **2009**, *96*, 5020−5029.

(3) Tamamis, P.; Kasotakis, E.; Mitraki, A.; Archontis, G. Amyloid-Like Self-Assembly of Peptide Sequences from the Adenovirus Fiber Shaft: Insights from Molecular Dynamics Simulations. *J. Phys. Chem. B* **2009**, *113*, 15639−15647.

(4) Tamamis, P.; Archontis, G. Amyloid-like Self-Assembly of a Dodecapeptide Sequence From the Adenovirus Fiber Shaft: Perspectives From Molecular Dynamics Simulations. *J. Non-Cryst. Solids* **2011**, *357*, 717−722.

(5) Gilead, S.; Gazit, E. Self-organization of Short Peptide Fragments: From Amyloid Fibrils to Nanoscale Supramolecular Assemblies. *Supramol. Chem.* **2005**, *17*, 87−92.

(6) Hauser, C. A. E.; Zhang, S. G. Designer Self-Assembling Peptide Nanofiber Biological Materials. *Chem. Soc. Rev.* **2010**, *39*, 2780−2790.

(7) Woolfson, D. N.; Mahmoud, Z. N. More than just Bare Scaffolds: Towards Multi-component and Decorated Fibrous Biomaterials. *Chem. Soc. Rev.* **2010**, *39*, 3464−3479.

(8) Colombo, G.; Soto, P.; Gazit, E. Peptide Self-Assembly at the Nanoscale: A Challenging Target for Computational and Experimental Biotechnology. *Trends Biotechnol.* **2007**, *25*, 211−218.

(9) Tsai, C. J.; Zheng, J.; Nussinov, R. Designing a Nanotube Using Naturally Occurring Protein Building Blocks. *PLOS Comput. Biol.* **2006**, *2*, 311−319.

(10) Luckey, M.; Hernandez, J. F.; Arlaud, G.; Forsyth, V. T.; Ruigrok, R. W. H.; Mitraki, A. A Peptide From the Adenovirus Fiber Shaft Forms Amyloid-type Fibrils. *FEBS Lett.* **2000**, *468*, 23−27.

(11) Mitraki, A.; Barge, A.; Chroboczek, J.; Andrieu, J. P.; Gagnon, J.; Ruigrok, R. W. Unfolding Studies of Human Adenovirus Type 2 Fibre Trimers: Evidence for a Stable Domain. *Eur. J. Biochem.* **1999**, *264*, 599−606.

(12) van Raaij, M. J.; Mitraki, A.; Lavigne, G.; Cusack, S. A Triple Beta-spiral in the Adenovirus Fibre Shaft Reveals a New Structural Motif for a Fibrous Protein. *Nature* **1999**, *401*, 935−938.

(13) Kasotakis, E.; Mossou, E.; Adler-Abramovich, L.; Mitchell, E. P.; Forsyth, V. T.; Gazit, E.; Mitraki, A. Design of Metal-Binding Sites Onto Self-Assembled Peptide Fibrils. *Biopolymers* **2009**, *92*, 164−172.

(14) Gazit, E. Use of Biomolecular Templates for the Fabrication of Metal Nanowires. *FEBS J.* **2007**, *274*, 317−322.

(15) Kasotakis, E.; Mitraki, A. Silica Biotemplating by Self-Assembling Peptides via Serine Residues Activated by the Peptide Amino Terminal Group. *Peptide Sci.* **2012**, *98*, 501−509.

(16) Gungormus, M.; Branco, M.; Fong, H.; Schneider, J. P.; Tamerler, C.; Sarikaya, M. Self Assembled Bi-Functional Peptide Hydrogels with Biomineralization-Directing Peptides. *Biomaterials* **2010**, *31*, 7266−7274.

(17) Hartgerink, J. D.; Beniash, E.; Stupp, S. I. Self-Assembly and Mineralization of Peptide-Amphiphile Nanofibers. *Science* **2001**, *294*, 1684−1688.

(18) Kirkham, J.; Firth, A.; Vernals, D.; Boden, N.; Robinson, C.; Shore, R. C.; Brookes, S. J.; Aggeli, A. Self-Assembling Peptide Scaffolds Promote Enamel Remineralization. *J. Dental Res.* **2007**, *86*, 426−430.

(19) Segman-Magidovich, S.; Grisaru, H.; Gitli, T.; Levi-Kalisman, Y.; Rapaport, H. Matrices of Acidic $\beta$-sheet Peptides as Templates for Calcium Phosphate Mineralization. *Adv. Mater.* **2008**, *20*, 2156−2161.

(20) Rapaport, H.; Grisaru, H.; Silberstein, T. Hydrogel Scaffolds of Amphiphilic and Acidic b-Sheet Peptides. *Adv. Funct. Mater.* **2008**, *18*, 2889−2896.

(21) Terzaki, K.; Kalloudi, E.; Mossou, E.; Mitchell, E. P.; Forsyth, V. T.; Rosseeva, E.; Simon, P.; Vamvakaki, M.; Chatzinikolaidou, M.; Mitraki, A.; Farsari, M. Mineralized Self-Assembled Peptides on 3D Laser-made Scaffolds: A New Route Towards 'Scaffold on Scaffold' Hard Tissue Engineering. *Biofabrication* **2013**, *5*, 045002.

(22) Addadi, L.; Weiner, S. Interactions Between Acidic Proteins and Crystals - Stereochemical Requirements in Biomineralization. *Proc. Natl. Acad. Sci. U.S.A.* **1985**, *82*, 4110−4114.

(23) Addadi, L.; Weiner, S. Control and Design Principles in Biological Mineralization. *Angew. Chem., Int. Ed. Engl.* **1992**, *31*, 153−169.

(24) Mann, S. *Biomineralization: Principles and Concepts in Bioinorganic Materials Chemistry*; Oxford University Press: New York, 2001.
(25) Hammersley, A. P. *FIT2D V9.129 Reference Manual V3.1*; ESRF Internal Report ESRF98HA01T; ESRF: Grenoble, France, 1998.
(26) Squire, J. M.; Al-Khayat, H.; Arnott, S.; Crawshaw, J.; Diakun, G.; Denny, R. C.; Dover, D.; Forsyth, V. T.; He, A.; Knupp, C.; Mant, G. R.; Rajkumar, G.; Rodman, M. J.; Shotton, M. S.; Windle, A. New CCP13 Software and the Strategy Behind Further Developments: Stripping and Modelling of Fibre Diffraction Data. *Fibre Diffr. Rev.* **2003**, *11*, 7−19.
(27) Brooks, B. R.; Brooks, C. L., III; Mackerell, A. D.; Nilsson, L.; Petrella, R. J.; Roux, B.; Won, Y.; Archontis, G.; Bartels, C.; Boresch, S.; et al. CHARMM: The Biomolecular Simulation Program. *J. Comput. Chem.* **2009**, *30*, 1545−1614.
(28) Seeber, M.; Felline, A.; Raimondi, F.; Muff, S.; Friedman, R.; Rao, F.; Caflisch, A.; Fanelli, F. ORDOM: A User-Friendly Program for the Analysis of Molecular Structures, Trajectories, and Free Energy Surfaces. *J. Comput. Chem.* **2011**, *32*, 1183−1194.
(29) Brooks, B. R.; Bruccoleri, R. E.; Olafson, B. D.; States, D. J.; Swaminathan, S.; Karplus, M. CHARMM: a Program for Macromolecular Energy, Minimization and Dynamics Calculations. *J. Comput. Chem.* **1983**, *4*, 187−217.
(30) Haberthür, U.; Caflisch, A. FACTS: Fast Analytical Continuum Treatment of Solvation. *J. Comput. Chem.* **2008**, *29*, 701−715.
(31) Felline, A.; Seeber, M.; Rao, F.; Fanelli, F. Computational Screening of Rhodopsin Mutations Associated with Retinitis Pigmentosa. *J. Chem. Theor. Comput.* **2009**, *5*, 2472−2485.
(32) Serquera, D.; Lee, W.; Settanni, G.; Marszalek, P. E.; Paci, E.; Itzhaki, L. S. Mechanical Unfolding of the Ankyrin Repeat Protein. *Biophys. J.* **2010**, *98*, 1294−1301.
(33) Tamamis, P.; Floudas, C. A. Molecular Recognition of CXCR4 by a Dual Tropic HIV-1 gp120 V3 Loop. *Biophys. J.* **2013**, *105*, 1502−1514.
(34) López de Victoria, A.; Tamamis, P.; Kieslich, C. A.; Morikis, D. Insights into the Structure, Correlated Motions, and Electrostatic Properties of Two HIV-1 gp120 V3 Loops. *PLoS ONE* **2012**, *7* (11), e49925.
(35) Khoury, G. A.; Tamamis, P.; Pinnaduwage, N.; Smadbeck, J.; Kieslich, C. A.; Floudas, C. A. Princeton_TIGRESS: Protein geometry refinement using simulations and support vector machines. *Proteins* **2013**, DOI: 10.1002/prot.24459.
(36) Ryckaert, J. P.; Ciccotti, G.; Berendsen, H. J. C. Numerical Integration of the Cartesian Equations of Motion of a System with Constraints: Molecular Dynamics of n-alkanes. *J. Comput. Phys.* **1977**, *23*, 327−341.
(37) Swendsen, R.; Wang, J. Non-universal Critical Dynamics in Monte Carlo Simulations. *Phys. Rev. Lett.* **1987**, *57*, 2607−2609.
(38) Sugita, Y.; Okamoto, Y. Replica-exchange Molecular Dynamics Method for Protein Folding. *Chem. Phys. Lett.* **1999**, *314*, 141−151.
(39) Sanbonmatsu, K. Y.; Garcia, A. E. Structure of Met-Enkephalin in Explicit Aqueous Solution Using Replica Exchange Molecular Dynamics. *Proteins: Struct., Funct., Genet.* **2002**, *46*, 225−234.
(40) Mackerell, A. D., Jr.; Bashford, D.; Bellott, M.; Dunbrack, R. L.; Evanseck, J. D.; Field, M. J.; Fischer, S.; Gao, J.; Guo, H.; Ha, S.; et al. An all-atom Empirical Potential for Molecular Modelling and Dynamics Study of Proteins. *J. Phys. Chem. B* **1998**, *102*, 3586−3616.
(41) MacKerell, A. D., Jr.; Feig, M.; Brooks, C. L., III. Extending the Treatment of Backbone Energetics in Protein Force Fields: Limitations of Gas-phase Quantum Mechanics in Reproducing Protein Conformational Distributions in Molecular Dynamics Simulations. *J. Comput. Chem.* **2004**, *25*, 1400−1415.
(42) Jorgensen, W. L.; Chandrasekhar, J.; Madura, J. D.; Impey, R. W.; Klein, M. L. Comparison of Simple Potential Functions for Simulating Liquid Water. *J. Chem. Phys.* **1983**, *79*, 926−935.
(43) Neria, E.; Fischer, S.; Karplus, M. Simulation of Activation Free Energies in Molecular Systems. *J. Chem. Phys.* **1996**, *105*, 1902−1921.
(44) Darden, T.; York, D.; Pedersen, L. Particle Mesh Ewald: An n log(n) Method for Ewald Sums in Large Systems. *J. Chem. Phys.* **1993**, *98*, 10089−10092.
(45) Nose, S. A Unified Formulation of the Constant Temperature Molecular Dynamics Method. *J. Chem. Phys.* **1984**, *81*, 511−519.
(46) Hoover, W. Canonical Dynamics: Equilibrium Phase-space Distributions. *Phys. Rev. A* **1985**, *31*, 1695−1697.
(47) Feller, S.; Zhang, Y.; Pastor, R. W.; Brooks, B. Constant-Pressure Molecular Dynamics Simulation: The Langevin Piston Method. *J. Chem. Phys.* **1995**, *103*, 4613−4621.
(48) Tamamis, P.; Skourtis, S. S.; Morikis, D.; Lambris, J. D.; Archontis, G. Conformational analysis of compstatin analogues with molecular dynamics simulations in explicit water. *J. Mol. Graphics Modell.* **2007**, *26* (2), 571−580.
(49) Kabsch, W.; Sander, C. Dictionary of Protein Secondary Structure: Pattern Recognition of Hydrogen-Bonded and Geometrical Features. *Biopolymers* **1983**, *22*, 2577−637.
(50) de Gennes, P. G.; Prost, J. *The Physics of Liquid Crystals*, 2nd ed.; Oxford University Press: Oxford, U.K., 1993.
(51) Allen, M. P.; Tildesley, D. J. *Computer Simulation of Liquids*; Oxford Science: Oxford, U.K., 1987.
(52) Doerr, T. P.; Heman, D.; Mathur, H.; Taylor, P. L. Randomness in Nanoscopic Liquid Crystal Droplets - How Small is Too Small? *Europhys. Lett.* **2002**, *59*, 398−402.
(53) Cecchini, M.; Rao, F.; Seeber, M.; Caflisch, A. Replica Exchange Molecular Dynamics Simulations of Amyloid Peptide Aggregation. *J. Chem. Phys.* **2004**, *121*, 10748.